Solution of the Structure of the High-Coverage CO Layer on the Ru(0001) Surface - a Combined Study by Density Functional Theory and Scanning Tunneling Microscopy

Hannah Illner[a)], Sung Sakong[b)], Axel Groß[b)], Joost Wintterlin[a),c)]*

[a)]Department of Chemistry, Ludwig-Maximilians-Universität München, 81377 Munich, Germany

[b)]Institute of Theoretical Chemistry, University of Ulm, 89081 Ulm, Germany

[c)]Center for NanoScience, Schellingstr. 4, 80799 Munich, Germany

*Corresponding author

Abstract

Structures formed by dense adsorbed CO layers can provide information about the balance between molecule-surface and molecule-molecule interactions. However, in many cases structure models are not clear. Using density functional theory (DFT) and scanning tunneling microscopy (STM) we have investigated the high-coverage CO layer on the Ru(0001) surface. Previous investigations by low-energy electron diffraction (LEED) and vibrational spectroscopy led to conflicting results about the structure. In the present study, 88 models with coverages between 0.58 and 0.77 monolayers have been analyzed by DFT. The most stable structures consist of small, compact CO clusters with an internal $(1\ x\ 1)$ structure. The CO molecules in the cluster centers occupy on-top sites in an upright position, whereas the molecules farther outside are slightly shifted from these sites and tilted outward. STM data of the CO-saturated surface at low temperatures, corresponding to a coverage of 0.66 monolayers, show a quasi-hexagonal pattern of features with an internal hexagonal fine structure. Simulated images based on the cluster model agree with the experimental data. It is concluded that the high-coverage CO layer consists of the close-packed clusters predicted by DFT as the most stable structure elements. In the experiment, sizes and shapes of the clusters vary. However, the arrangement is not random but follows defined tiling rules. The structure remains ordered almost up to room temperature. The LEED data are re-interpreted on the basis of the Fourier transforms of the STM data, solving the long-standing conflict about the structure.

Introduction

Dense layers of adsorbed CO molecules on transition metal surfaces show, in an exemplary way, how the structure of an adsorption layer can be determined by counteracting molecule-surface and molecule-molecule interactions. The CO-metal bond is relatively strong and the molecules preferentially bind to defined adsorption sites, but it is not strong enough to prevent displacements from these sites when repulsive interactions between neighboring molecules become important. At high coverages these two interactions have to be balanced in some way.

On the hexagonally close-packed surfaces of the fcc and hcp transition metals, the preferred CO binding positions are the high-symmetry sites on-top, bridge, hcp threefold hollow, and fcc threefold hollow. Which site is most favored depends on the metal. However, the size of the CO molecule prevents that all sites of the same type can be occupied at the same time, and coverages (Θ) of one monolayer (ML, in units of CO molecules per metal surface atom) cannot be reached. The size of CO, approximately its van-der-Waals diameter, can be estimated from the saturation coverages of CO on the Co(0001) and Pt(111) surfaces, giving values between 3.11 and 3.36 Å.[1, 2] These values are, in all cases, higher than the spacings between equivalent adsorption sites which are given by the lattice constants of the surfaces. The resulting restrictions for the arrangements of the molecules give rise to a rich variety of different high-coverage structures on the (0001) or (111) surfaces of Co, Ni, Cu, Ru, Rh, Pd, Ir, and Pt.[3] Which structure is formed in a given case is determined by the electronic structure and lattice constant of the metal and by the exact CO coverage. However, recent theory work found very low energy differences between different high-coverage structures, indicating that predictions about a structure are difficult.[4]

What can be done is to classify the high-coverage CO structures on these surfaces according to common construction principles. Four types of models can be identified: (1) Models with mixed adsorption sites. In these models, one fraction of molecules occupies their most preferred sites whereas a second fraction occupies "second-best" sites in between. CO-metal interactions still dominate. Examples are the $c(4\ x\ 2)$ CO structure on Pt(111) (Θ = 0.50 ML) and the $\left(\sqrt{7}\ x\ \sqrt{7}\right)R19°$ structure on Ni(111) (Θ = 0.57 ML).[5, 6] (2) Moiré models. In these models, the CO molecules form hexagonally close-packed layers with larger lattice constants than the underlying metal. The mismatch of the two lattices gives rise to a moiré effect. Repulsive interactions between the CO molecules dominate. Most of the early low-energy electron diffraction (LEED) studies on the hexagonally close-packed metal surfaces have assumed such models. Cases confirmed by scanning tunneling microscopy (STM) are the CO layers on Pt(111) at Θ = 0.51 to 0.68 ML at 300 K and on Co(0001) at Θ = 0.63 to 0.65 ML at 300 K.[1, 2] (3) Antiphase domain boundary models.[3, 7] In these models, the CO molecules form narrow, one-dimensionally extended domains with a simple or mixed site internal structure in which all CO molecules occupy high-symmetry sites. The domains are separated by "heavy domain walls" with a denser CO packing. There is also the inverse case, dense domains separated by light domain walls. CO-metal interactions dominate. Such structures have been observed for Pt(111) and Co(0001) at low temperatures.[8, 9] (4) Cluster models. In these models the molecules form small islands with an internal $(1\ x\ 1)$ structure. CO-metal interactions dominate, and all molecules are on, or close to, high-symmetry sites. Repulsive interactions within the clusters limit the cluster sizes to a few molecules. Examples are the $\left(3\sqrt{3}\ x\ 3\sqrt{3}\right)R30°$ structure on Ir(111) at Θ = 0.70 ML and the $\left(2\sqrt{3}\ x\ 2\sqrt{3}\right)R30°$ structure on Ru(0001) at Θ = 0.58 ML.[10-12]

CO layers on Ru(0001) at higher coverages than 0.58 ML do not seem to fit into this classification. Early LEED experiments showed diffraction patterns at coverages between Θ = 0.58 and 0.65 ML (0.66 ML) [fig. 1(a)] that clearly pointed to moiré structures (at that time termed compressed or hexagonal phases).[13, 14] Arguments for moiré structures are, firstly, that the most intense diffraction spots of the adsorption layer (reciprocal lattice vectors $\vec{h}_1^{\mathrm{CO}}$, $\vec{h}_2^{\mathrm{CO}}$, and symmetry equivalents) close to the first order diffraction spots of the Ru substrate (reciprocal lattice vectors $\vec{g}_1^{\mathrm{Ru}}$, $\vec{g}_2^{\mathrm{Ru}}$, and symmetry equivalents) can, in a straightforward manner, be explained by diffraction at a hexagonal, rotated layer of CO molecules with a larger lattice constant than the substrate [fig. 1(b)]. The fact that the superstructure spots appear as pairs can be accounted for by the two possible rotational domains. The six superstructure spots close to the origin can be explained by multiple scattering. Secondly, when the CO coverage was increased from Θ = 0.58 to 0.65 ML (0.66 ML), the superstructure spots continuously shifted toward the nearest substrate spots.[13, 14] This is exactly what is expected for a moiré structure that is compressed when it adopts additional molecules. Thirdly, for a hexagonally close-packed CO layer one expects that saturation is reached when the lattice constant of the layer gets close to the van-der-Waals diameter of CO. Using the saturation coverage of 0.66 ML, a value determined independently of a structure model,[14] the moiré model gives a CO-CO distance of 3.33 Å. This value is, in fact, in the range of the van-der-Waals diameters of CO.

On the other hand, high-resolution electron energy loss spectroscopy (HREELS) and reflection absorption infrared spectroscopy (RAIRS) showed one vibrational C-O mode only, over the entire range of coverages up to saturation.[15, 16] The peak displayed some shift with increasing coverage which can be explained by dipole-dipole coupling and an additional weakening of the CO-metal bond,[17, 18] but it remained in the range of on-top-bonded CO. This observation is in obvious contradiction to moiré structures which contain CO molecules on all kinds of sites [fig. 1(b)].

There have been ideas how this discrepancy can be resolved. One has been that the vibrational spectra may have to be interpreted differently. The observed C-O mode may, in general, not exclusively mark on-top CO,[15] or, at least in a situation where molecule-molecule interactions dominate, it may no longer be valid to attribute a certain vibrational C-O frequency to a certain binding site.[16] Another idea has been that the LEED pattern can alternatively be interpreted by an antiphase domain boundary model.[3] In this model, CO molecules would form long, narrow domains with an internal $(1\ x\ 1)$ structure, in which all molecules occupy on-top positions. Domain boundaries formed by empty Ru sites would allow for relaxations perpendicularly to the domains. There would be three rotational domains, and the superimposed diffraction patterns from these domains would give the same LEED pattern as the one shown in fig. 1(a). Monte-Carlo simulations supported this model.[19] Observations by electron stimulated desorption ion angular distribution (ESDIAD) that the molecular axes at saturation are tilted from the surface normal by a few degrees can be explained by the relaxations expected for such a model.[20] However, a recent STM investigation of CO/H coadsorbed layers on Ru(0001) was in disagreement with the antiphase domain model.[21] Images recorded at a high CO coverage, where H was most likely absent, showed some hexagonal pattern rather than the one-dimensional features one would expect. No structure model was proposed.

Here we present an investigation of the high-coverage CO layer on Ru(0001) by density functional theory (DFT) and STM. Fourier transformations of the STM data are used for comparison with the LEED pattern. We find a structure model that is in agreement with all previous experimental observations. In particular, it solves the seeming conflict between the vibrational spectroscopy and the LEED data.

Experimental Section

The experiments were performed in an ultra-high vacuum (UHV) chamber (base pressure <1 × 10^{-10} mbar) by means of a home-built, beetle-type scanning tunneling microscope. With this setup, sample temperatures can be varied between 50 and 500 K by a liquid He flow cryostat that cools the sample holder of the STM, and by simultaneous radiative heating from a filament at the back of the sample. Details of the setup have been described previously.[22] Images were recorded in the standard, slow constant current mode and also in the fast constant height mode. For the present analysis we do not make use of the high time resolution of this mode. The chamber was additionally equipped with an Auger electron spectrometer (AES), a low-energy electron diffraction optics, an ion gun, a quadrupole mass spectrometer, and a sample manipulator.

For preparation, the Ru(0001) sample was repeatedly sputtered, annealed, oxidized, and annealed again. The sample was first sputtered with 1 keV Ar ions for 10 to 15 min and then flash-annealed to 1470 K. Residual carbon was then oxidized by dosing O_2 in various amounts. For higher amounts of carbon, the chamber was backfilled with 2 × 10^{-7} mbar of O_2 for 10−15 min at 910 K. For lower carbon coverages, dosing 2 − 20 L of O_2 at 298−423 K was sufficient [1 Langmuir (L) = 1.33 × 10^{-6} mbar s]. To react off the carbon and desorb excess oxygen the sample was flash-annealed to 1700 K. This sequence was repeated until AES showed a clean sample. The problem with AES of the overlapping carbon KLL peak at 272 eV with the Ru MNN peak at 273 eV was solved by the known procedure to use the asymmetry of the overlapped peaks as a measure of the carbon coverage.[23-25] Directly before an experiment, the sample was shortly annealed to 623 K to desorb any molecules that had adsorbed in the time period after the last high-temperature flash. Then the sample was transferred to the STM.

High coverages of CO were prepared in two steps. First, 50 L of CO were dosed on the freshly prepared surface at a temperature slightly above 300 K. This treatment led to an incomplete $\left(2\sqrt{3}\ x\ 2\sqrt{3}\right)R30°$ structure, the CO structure described in a recent publication.[12] The coverage of Θ = 0.47 ML of this structure is close to the saturation coverage attainable by dosing CO at room temperature. This procedure was used to protect the surface, by means of the CO layer, against adsorption of foreign gases, mainly H_2 and H_2O, when the sample cooled to the measurement temperature. In a second step, additional 15 L of CO were dosed while the sample cooled from room temperature to 60−70 K. In this way a coverage of 0.66 ML of CO was obtained. In an additional STM experiment, the temperature was enhanced in steps to room temperature to detect possible phase transitions.

Setup of the density functional theory calculations

The VASP software package was used to compute the adsorption energy of the CO adlayer on the Ru(0001) surface based on periodic DFT.[26] The revised version of the Perdew-Burke-Ernzerhof (RPBE) functional was employed to account for exchange-correlation effects.[27] The electronic wave functions were expanded in a plane-wave basis set up to an energy cutoff of 350 eV. The ionic cores were taken into account by the projector augmented wave (PAW) potential.[28] Dispersion interactions between the CO molecules and the first layer of the Ru slab were computed by the D3 correction scheme of Grimme et al.[29] Note that the RPBE+D3 approach employed here has been shown to yield rather reliable molecular adsorption energies.[30]

We modeled the Ru(0001) surface using a slab consisting of three atomic layers. For the Ru hcp bulk structure, lattice parameters of a = 2.74 Å and c/a = 1.58 were obtained, in good agreement with the experimental values a = 2.706 Å and c/a = 1.58. The CO molecules were placed at on-top sites in all investigated structures which are more stable than the hcp hollow, fcc hollow, and bridge sites by 0.30, 0.34, and 0.32 eV, respectively. These values are only little affected by the presence of CO molecules on neighboring on-top sites. Relaxations from the exact on-top positions were allowed, but structures with other CO positions were not considered.

A first set of structures was formed by clusters consisting of 7, 10, 12, 14, 16, and 19 CO molecules, all bonded at on-top positions (fig. 2, a further configuration with 37 CO molecules is not shown) and separated by rows of uncovered Ru atoms (unit cells are marked). The first Brillouin zones of these configurations were integrated using 6 x 6, 6 x 6, 3 x 3, 5 x 5, 3 x 3, 4 x 4, and 2 x 2 k-point meshes for the corresponding surface unit cells. In all cases we optimized the energy minimum configurations by relaxing the topmost Ru layers of the slabs and the CO molecules until the forces were converged to 0.01 eV/Å. Periodic images of the slab were separated by vacuum layers of 15 Å, and dipole corrections were applied to compensate any dipole field between the periodic images.

In addition to the cluster configurations, we considered further CO adlayer configurations on a $\left(4\sqrt{3}\ x\ 4\sqrt{3}\right)R30°$ unit cell, corresponding to a coverage variation from 0.58 to 0.77 ML. We also added CO molecules into the configuration consisting of 7 CO clusters and displaced CO molecules from their positions in the clusters. Finally, we considered configurations with CO vacancies in a honeycomb structure (0.75 ML) to probe a possible adlayer phase change from a $\left(2\sqrt{3}\ x\ 2\sqrt{3}\right)R30°$ cluster structure to a $(2\ x\ 2)$ honeycomb structure. Altogether, 88 structures were analyzed.

The relative adsorption energy of CO adlyers (E_{ads}) was computed with respect to the adsorption energy of an isolated CO molecule on the clean Ru(0001) surface:

$$E_{ads} = \frac{E_{tot} - E_{\mathrm{Ru(0001)}} - n_{\mathrm{CO}} E_{\mathrm{CO}}}{n_{\mathrm{CO}}} \qquad (1)$$

E_{tot} is the total energy of the CO adlayer on the Ru surface, $E_{\mathrm{Ru(0001)}}$ is the energy of the clean Ru(0001) slab, E_{CO} is the energy of a single CO molecule on the Ru surface given by the sum of the energy of a CO molecule in the gas phase and its adsorption energy of -1.92 eV, and n_{CO} is the number of the CO molecules in the unit cell. Because of the repulsions between the adsorbed CO molecules all E_{ads} values at finite coverages are positive.

We have also performed simulations of constant height STM images using the Tersoff-Hamman approximation.[31] For this purpose, densities of states were integrated over the energy ranges 0.0 eV (the Fermi energy) to -0.2, -0.4, -0.5, -0.8, and -1.0 eV. The negative signs, which reflect the negative tunneling voltages (V_t) chosen in the experiments, correspond to occupied states. The charges were calculated in steps of 0.1 Å above the uppermost O atoms in a range from 1.6 to 3.6 Å, and the resulting charge grids were then linearly interpolated to compute the images. Good agreement with the experimental constant height images was obtained for the integration range 0.0 to -1.0 eV and a distance of 2.5 Å. The experiments only showed minor variations of the contrast between V_t = -0.2 and -1.6 V, and we note that the absolute tunneling distance is not an experimentally available parameter.

Results and discussion

DFT calculations

We first present the high-coverage structure models analyzed by DFT, and then compare these models with the STM data. The calculations were numerically demanding because of the relatively large unit cells and the correspondingly high number of molecules in the cells. An analysis of all possible CO configurations was therefore not feasible. To reduce the number of possibilities, we used the $\left(2\sqrt{3}\ x\ 2\sqrt{3}\right)R30°$-CO structure (Θ = 0.58 ML) for which a validated structure model exists, to define elements that a stable high-coverage structure most likely contains. The $\left(2\sqrt{3}\ x\ 2\sqrt{3}\right)R30°$ structure belongs to the class of cluster models mentioned above.[11, 12] It is formed by clusters consisting of seven CO molecules, one central molecule in an upright position, and a ring of six surrounding molecules that are slightly tilted away from the center [fig. 2(a)]. Rows of CO-free Ru atoms separate these clusters. At the junctions of three empty Ru rows, three CO molecules form triangles with $\sqrt{3}a$ long edges [blue mark in fig. 2(a)]. We find that these triangle configurations significantly contribute to the local stability of the structure. This can be seen, e.g., by the 0.22 eV energy increase when a CO molecule is moved from the triangular edge of the 7 CO cluster to the center of the triangle. The $\left(2\sqrt{3}\ x\ 2\sqrt{3}\right)R30°$ structure is quite stable, and one can remove several CO molecules without destabilizing it. For example, the CO structure at Θ = 0.47 ML is formed from CO-deficient clusters but still follows the same construction principle.[12]

To model the CO layer at higher coverages than 0.58 ML the following assumptions were made: CO molecules exclusively occupy the on-top sites at all coverages, a condition based on the corresponding findings by vibrational spectroscopy.[15, 16] When the coverage is increased, the layer maintains a cluster structure but the internal structures and/or the sizes of the clusters change. The clusters are separated by one-atom-wide rows of unoccupied, or only partially occupied, Ru atoms. These non-covered Ru sites allow the molecules to relax the stress in the densely packed clusters. Larger empty areas are not permitted. The CO triangles at the junctions of the empty rows are preserved in all models, which puts limits on possible arrangements, sizes, and shapes of the clusters. When upon a coverage change a new distribution of junctions becomes energetically favored, the CO molecules are assumed to regroup immediately; kinetic restrictions are not considered because of the low hopping barrier of CO. 88 CO configurations were investigated in the coverage range from 0.58 to 0.77 ML and tested for their stabilities; energies are plotted in fig. 4 as a function of the CO coverage. At a given CO coverage, a configuration with lower relative adsorption energy [eq. (1)] corresponds to a more likely structure.

We probed the energetics of three types of models that satisfy the mentioned assumptions. The first type of models consists of compact clusters of increasing size. Figures 2(a) to (f) show the first six of these configurations, with clusters consisting of 7, 10, 2x12+7, 14, 2x16+10, and 19 CO molecules, with internal $(1\ x\ 1)$ configurations in all cases. The models correspond to coverages between Θ = 0.58 and 0.70 ML. Models only consisting of 12-CO or 16-CO clusters cannot be constructed within the given constrictions, and one 7-CO or 10-CO cluster, respectively, have to be added to the unit cells. A model with 37-CO clusters (Θ = 0.77 ML) has also been considered; it was formed from the 19-CO cluster model by adding a complete ring of CO molecules around the 19-CO clusters (not shown).

After optimization, the DFT calculations show that, except for the CO molecules at the cluster centers, the molecules are no longer exactly on-top of the Ru atoms. The C atoms are displaced from the centers of the Ru atoms by distances that increase with the size of the clusters to a value of 0.7 Å. There are

also deviations of the molecular axes from the surface normal. The molecule at the center of a cluster is in an upright position, but the surrounding molecules are tilted outward by an angle that increases with increasing distance from the cluster center. The maximum tilt at the rims is 16°. Shifts and tilts are caused by the dense $(1\ x\ 1)$ packing of the CO molecules in the clusters. Figure 4 shows the relative energies of these models (pink hexagons). The energy increases almost linearly with coverage, which reflects the increasing average repulsion with increasing cluster size.

The data contain information about the question whether the relative positions of the triangles, which are formed by the CO molecules at the edges of the clusters, play a role. As one can see in fig. 2, each model of this type has a different periodicity of CO triangles. On the other hand, two pairs of different models almost have the same CO coverages. The 2x12+7- and the 10-CO models have CO coverages of 0.633 and 0.625 ML, and the 2x16+10 and the 14-CO models even have identical CO coverages of 0.667 ML. The coverages of triangles are also almost pairwise identical, 0.122 and 0.125 ML for the 2x12+7- and the 10-CO models, and 0.095 ML for the 2x16+10- and the 14-CO models. Figure 4 shows that these pairs of models almost have the same energy. This fact shows that the stabilities of the models of this type are mainly determined by the overall CO coverages. It does not play a significant role whether the model contains clusters of one size or of two different sizes and how the triangles are arranged with respect to each other. The effect of the CO triangles is a local one; it does not extend to the nearest neighbor triangle.

The second type of models is based on interstitial CO molecules in the $\left(2\sqrt{3}\ x\ 2\sqrt{3}\right)R30°$-CO structure. In these models, the 7-CO clusters were kept at their original positions, and additional CO molecules were filled in. The simulations were performed on $\left(4\sqrt{3}\ x\ 4\sqrt{3}\right)R30°$ unit cells that contain four of the 7-CO clusters. Figures 3(a) to (c) show configurations created by adding one, two, and three CO molecules to this cell. The additional molecules occupy sites on the empty Ru rows where they have four CO neighbors. In this way bridges between neighboring clusters are formed. Various configurations of this type were explored by moving the added CO molecules between the empty Ru sites. The positions of the 7-CO clusters were left unchanged. To create higher coverages, the sites inside the CO triangles were also occupied. In this way, the number of connected clusters is minimized, and new larger clusters are created. The resulting larger clusters mostly appear in triangular shapes with concave edges.

Figure 4 (blue squares) shows that, for each coverage, the energies of the models of this second type vary depending on the exact local configurations. At coverages below 0.63 ML, the most stable configurations are energetically comparable to the first type of models (pink hexagons) at the same coverages. Hence, adding a small number of CO molecules to the $\left(2\sqrt{3}\ x\ 2\sqrt{3}\right)R30°$-CO structure does not necessarily lift the 7-CO cluster structure. However, as the coverage is increased to ≥0.67 ML, all considered structures based on the 7-CO cluster model become less stable than the structures based on the compact larger clusters.

The third type of models is based on a $(2\ x\ 2)$-CO structure in which the CO molecules form a honeycomb network of open rings, corresponding to a coverage of 0.75 ML [fig. 3(d)]. To derive models from this structure, CO molecules were removed, and the remaining molecules were rearranged to form clusters with an internal $(2\ x\ 2)$ structure. Like for the other two model types, the clusters were arranged such that their edges form CO triangles. Again a $\left(4\sqrt{3}\ x\ 4\sqrt{3}\right)R30°$ simulation cell was used. An example with seven open rings inside the clusters is shown in fig. 3(e) (Θ = 0.63 ML). It is found that

all configurations derived from this model type are less stable than the other two models (fig. 4, green diamonds). The cluster considers a possible configuration of the long-range order of $\left(4\sqrt{3}\ x\ 4\sqrt{3}\right)R30°$ with a $(2\ x\ 2)$ internal structure. Vacancies in the $(2\ x\ 2)$ matrix just cause CO disorder in the whole simulation cell, whereas a symmetric distribution of CO vacancies can lead to a cluster configuration. We have also modified the internal structure of the clusters by replacing the $(2\ x\ 2)$ rings by CO triangles [fig. 3(f)], which leads to intermediate models between the third and the first type. These structures are more stable than those with $(2\ x\ 2)$ rings, and they can be further stabilized by shifting CO molecules to new sites, locally restoring 7-CO clusters. The energies (fig. 4, orange dots) become then similar to those of the 7-CO cluster models.

However, when one considers the full range of coverages from 0.58 to 0.77 ML, the models formed by compact clusters have the lowest energies.

STM results

Figure 5(a) shows an STM image of the high-coverage CO layer recorded at 62 K in the standard constant current mode. One can see structure elements of various sizes arranged in a partially ordered hexagonal pattern with a periodicity of approximately 12 Å. The rows of structure elements are roughly aligned to the $\sqrt{3}$ directions of the Ru surface, but because of the uneven sizes and shapes of the features, the rows are not exactly straight, and the directions of the rows deviate by small angles from the crystallographic $\sqrt{3}$ directions. The features themselves display an internal fine structure of dark dots, the numbers of which vary from one for the smallest feature to seven for the largest (one is marked red). Figure 5(b) shows that the dark dots inside the features form a hexagonal structure; spacings are 3.3 Å and directions are the close-packed directions of the Ru surface.

A moiré structure can be ruled out by these observations. Moiré structures would display extended hexagonal, periodic patterns superimposed by a continuous hexagonal fine structure. The actually observed structure is only poorly ordered and the hexagonal fine structure is restricted to the interiors of the features, which is in conflict with this expectation. Likewise, antiphase domain boundary models can be ruled out. Regardless of the exact arrangements of the CO molecules in such a model, STM images would display extended one-dimensional features rather than the quasi-hexagonal pattern actually seen.

The general appearance of the STM data suggests a cluster model. Of the three types we have investigated by DFT we can rule out models with interstitial CO molecules in the preserved $\left(2\sqrt{3}\ x\ 2\sqrt{3}\right)R30°$-CO structure. The $\left(2\sqrt{3}\ x\ 2\sqrt{3}\right)R30°$ lattice is clearly lifted. Cluster models with internal $(2\ x\ 2)$ or $\sqrt{3}$ structures are in conflict with the observed $(1\ x\ 1)$ fine structure. The only remaining model is the first type that consists of compact clusters with an internal $(1\ x\ 1)$ structure. If this model is correct, the dark dots within the structure elements would represent the innermost CO molecules of the clusters and the dark spaces between the features the more strongly tilted molecules at the rims.

To test this interpretation, we have simulated constant-height STM images. An experimental constant-height image is shown in fig. 6 (center). It was recorded with a negative tunneling voltage, which, in the constant-height mode, leads to an inverted contrast from the images recorded in the constant-

current mode (fig. 5). Accordingly, the fine structure in the features is formed by bright dots and the spaces between the features by almost continuous bright stripes.

The panels around the STM image are the simulated constant-height images from the six cluster models of fig. 2, also with inverted contrast. Considering, e.g., the simulated image of the 19-CO model, one can see structure elements with seven internal bright dots and bright, almost smooth spacings between the elements. The internal bright dots are at the positions of the seven innermost CO molecules, and the bright space is close to the positions of the 12 tilted outer molecules. The rows of unoccupied Ru atoms between the clusters do not give any additional contrast. In the experimental image, the same structure elements, with seven bright dots and bright spacings can be found, which can therefore be interpreted as 19-CO clusters (see mark). These are the largest elements observed. Similarly good agreement between the simulations and the experiment is found for the smaller clusters of the five other configurations in fig. 2 and the structure elements in the STM. Almost all features in the experiment have corresponding counterparts in the simulations. This agreement is strong evidence that the model of compact $(1\ x\ 1)$ clusters, with relaxed positions and tilting angles of the molecules, describes the structure correctly.

Figure 7 shows the resulting structure model for a section of the STM image in fig. 6 (black rectangle). Quite clearly, the high-coverage CO structure on Ru(0001) belongs to the class of cluster models, like the $\left(3\sqrt{3}\ x\ 3\sqrt{3}\right)R30°$ structure on Ir(111) and the $\left(2\sqrt{3}\ x\ 2\sqrt{3}\right)R30°$ structure on Ru(0001).[10, 11] However, in contrast to an ideal cluster model, the clusters on Ru(0001) display distributions of sizes and orientations, and their arrangements are not exactly periodic. Nevertheless, the configurations of the clusters are not random but follow strict "tiling rules". There is only a limited set of different clusters, and the relative orientations are such that between two neighboring clusters a one atom-wide row of empty Ru atoms is left. At the edges between three neighboring clusters the CO molecules form triangle configurations. In the entire area of fig. 7, there are only few locations where the edges do not form such triangles (one is marked orange), and just there the STM shows instabilities, probably caused by site exchanges of CO molecules. This model is in agreement with all previous findings: The molecules only occupy on-top sites in agreement with the vibrational spectra;[15, 16] most of the molecules are tilted which agrees with the ESDIAD data;[20] and the CO saturation coverage, determined by counting the clusters in the STM images, is 0.66 ML, in good agreement with the previously measured values of 0.65 and 0.66 ML.[13, 14]

To test the stability of the structure, the temperature was raised in steps of approximately 30 K starting at 62 K up to room temperature. Until 281 K the structure was continuously well resolved by the STM, without any enhanced fluctuations of the cluster features. At 298 K the structure had disappeared, most likely because a fraction of the CO layer had desorbed. These observations contrast with our previous experiments on the partial $\left(2\sqrt{3}\ x\ 2\sqrt{3}\right)R30°$-CO structure,[12] which showed a defined structure at 70 K, but structureless images at $T \geq 239$ K, although no CO has been lost by desorption. This fact was explained by the order-disorder transition observed in previous LEED experiments,[14] connected with an enhanced mobility of the molecules. The high-coverage structure of the present study does not undergo such an order-disorder transition, which also agrees with previous LEED results.[14]

A previous study by near-ambient pressure X-ray photoelectron spectroscopy (NAP-XPS) indicated that at 300 K under a constant CO pressure of 1 Torr, a bridge-bonded CO might exist on Ru(0001), in

addition to the on-top CO.[32] In our experiments, a temperature of 300 K could not be adjusted without desorbing part of the CO, so that we cannot comment on such a possibility.

Simulations of the diffraction pattern

What remains to be clarified is the interpretation of the LEED data. As mentioned in the introduction, the LEED pattern had suggested a moiré structure.[13, 14] To make sure that the CO layer in our experiments is comparable with these studies, we have performed some own LEED measurements. CO was dosed like in the STM experiments in two portions, the first at room temperature, the second during cooling, and only the final temperature was not as low because the sample, which was mounted to the manipulator in these experiments, was cooled by liquid N_2 instead of He. Figure 8 shows the LEED pattern at 150 K. One can see two broad diffraction spots close to the Ru substrate spots, at the same positions as in the schematic LEED pattern of fig. 1(a).[13, 14] It can be concluded that we have prepared the same structure.

To simulate the LEED pattern, we Fourier-transformed our STM data; fig. 9(a) shows the result for the STM image of fig. 6. One can see a hexagonal, periodic pattern of spots around the origin that represent the first Fourier components of the quasi-hexagonal configuration of the cluster features. However, the outermost six groups of pairs of spots (one group is marked) are different; they are somewhat displaced with respect to the (reciprocal) lattice one can construct from the inner spots.

To better understand these displacements, we constructed a strongly simplified model of the STM image and then Fourier-transformed this model (fig. 10). The model consists of simple dots drawn at the positions of the internal hexagonal features of the clusters in fig. 6. Figure 10(a) shows the positions as black dots. The atoms of the Ru surface are not visible in the STM image, but the substrate lattice (blue dots) can be constructed using other observations. From the lattice constant of Ru (2.706 Å) and the periodicity of the fine structure of the clusters (3.3 Å), we know that the substrate lattice constant should be 82% of the spacings between the black dots. The rotational angle of the Ru lattice with respect to the STM image we know from previous experiments with the $\left(\sqrt{3}\ x\ \sqrt{3}\right)R30°$-CO structure and from the orientation of the internal fine structure of the clusters. And the lateral relative positions of the blue and black dots we know from the fact that the centers of the clusters should be on top of the Ru atoms. As shown in fig. 10(a), with the substrate lattice constructed in this way, the center dots of most of the clusters, in fact, pretty well fall on positions of blue dots.

This model was then Fourier-transformed, in one case [fig. 10(b)] by using the black dot pattern only, without the blue dots, which reflects the actual situation in the STM image, and in the other case by using the superposition of both dot patterns [fig. 10 (c)]. Somewhat surprisingly at first glance, the two Fourier transforms are very similar. Only the spot intensities are different. In both cases the Fourier transforms show hexagonal patterns of spots from the substrate lattice and satellite spots around the substrate spots from the quasi-hexagonal cluster configuration. That there are substrate spots in fig. 10(b), despite the absence of the blue dot pattern, can be understood by the fact that the spacings between the cluster centers are multiples of lattice spacings of the substrate [fig. 10(a)]. The Fourier transform therefore contains components of the substrate.

In fig. 10(d) grids of lines are drawn through the positions of the spots. Blue lines run through the substrate spots, red lines through the satellites around the origin, and green hexagons mark the first

order satellites around the substrate spots. One can see that the first order substrate spots (crossing points of the blue lines) together with their satellites (green hexagons) do not coincide with the grid of the red lines.

One could successively superimpose finer grids than the red one to make the spots finally coincide with such a grid. In real space, this would correspond to successively larger periodicities comprising several clusters. This method has been applied to construct the unit cells of CO moiré structures on the Co(0001) surface.[33] However, after applying the first two finer grids, small displacements still remain. In such a case, when small but significant displacements from periodic lattices remain after applying successively finer grids, an effect also known from moiré structures,[33] the corresponding structure is practically incommensurate. For the present system, this is actually an unexpected result. Incommensurate superstructures are usually associated with moiré structures which are determined by intra-layer interactions, so that the registry with the surface is less important. Here, CO forms an incommensurate superstructure although all molecules are in approximate registry with the substrate. The (average) incommensurability results from the fact that the clusters display a distribution of sizes and shapes.

We then transferred the line grids constructed in fig. 10(d) to the Fourier transform of the experimental image [fig. 9(b)], without any adjustments except for the overall size. Perfect matching with the spots is found, confirming that the dot pattern in fig. 10(a) describes the order in the STM image well. The displaced green hexagons around the first order substrate spots in fig. 9(b) fall on the outer six groups of spot pairs, showing that these spots come from the incommensurate, quasi-hexagonal arrangement of the clusters. These spot pairs contain a considerable amount of information about the structure; Fourier back transformation of the 12 spots, with small windows around them, provides a real-space image [fig. 9(c)] that already contains major features of the actual STM image (fig. 6).

With this analysis, re-interpretation of the LEED pattern is straightforward. The pairs of the most intense superstructure spots close to the first order substrate spots [fig. 1(a)] are not caused by diffraction at a periodic hexagonal CO layer, which does not exist in the cluster model. In the cluster model, these spots are caused by multiple scattering at the substrate ($\vec{g}_i^{\mathrm{Ru}}$) and the quasi-hexagonal lattice of the clusters ($\vec{h}_j^{\mathrm{cluster}}$), see fig. 10(d). The six spots around the origin are caused by scattering at the cluster lattice only ($\vec{h}_j^{\mathrm{cluster}}$). The ratio of the lengths of vectors, $\left|\vec{h}_j^{\mathrm{cluster}}\right|/\left|\vec{g}_i^{\mathrm{Ru}}\right|$, as extracted from the Fourier transform, varies somewhat around 0.22 depending on directions. This value is close to the value of 0.23 for a perfect $\left(5\sqrt{3}\ x\ 5\sqrt{3}\right)R30°$ structure, the structure proposed on the basis of the LEED pattern.[13] However, the small difference is significant and a result of the fact that the actual structure is incommensurate. The reported continuous shifts of the LEED spots with varying CO coverage[13, 14] can also be explained by the incommensurability. Finally, the large width of the LEED spots can be explained by the ill-defined periodicity of the structure that leads to variations across the macroscopic surface area illuminated by the LEED beam.

Conclusions

In this study, high-coverage structures of CO on the Ru(0001) surface have been investigated by means of DFT and STM. 88 structure models of three different types, with coverages between 0.58 and 0.77 ML, have been analyzed by DFT. In all models the CO molecules occupy on-top sites. We find that the most stable type of models consists of clusters formed by compact, small islands of 7 to 37 CO

molecules with an internal $(1\ x\ 1)$ structure. The clusters are separated by rows of empty Ru atoms which allow the molecules to lower the repulsive interactions by relaxations. In all structures, the clusters are arranged such that three CO molecules at the edges between three clusters form triangles with $\sqrt{3}a$ long edges. This structure element considerably contributes to the stability of the structures. The CO molecules in the centers of the clusters are exactly on top of the Ru atoms and bonded in an upright position whereas the outer molecules are shifted from the Ru atoms, by up to 0.7 Å, and have tilted molecular axes by up to 16°.

STM data were recorded after saturating the surface with CO at temperatures between 60 and 70 K. The images show approximately hexagonal configurations of features with an internal hexagonal fine structure. STM images were simulated by applying the Tersoff-Hamann approximation to the most stable model,[31] and good agreement with the features observed by STM was found. The features can therefore be interpreted as the CO clusters predicted by DFT. The internal $(1\ x\ 1)$ fine structure can be interpreted as the innermost CO molecules, and the smooth spacings between the clusters as the CO molecules at the rims. In the experiment, the clusters display a distribution of sizes ranging from 7- to 19-CO clusters, and, as a consequence, the configuration is not exactly hexagonally ordered. However, the arrangement is not random but governed by tiling rules that determine the relative orientations of the clusters, namely that one-atom-wide empty rows have to be left between the clusters and that the edges have to be formed by CO triangles. STM annealing experiments showed that the structure remains ordered up to 281 K.

The on-top positions of the molecules in the model agree with results of previous HREELS and RAIRS studies.[15, 16] The tilting of the molecules agrees with observations by ESDIAD,[20] and the saturation coverage of 0.66 ML agrees with the previously reported values.[13, 14] The Fourier transform of the STM data shows spots at the positions of the most intense superstructure spots observed in previous LEED investigations and reproduced in the present study.[13, 14] According to the cluster model, these spots are not caused by diffraction at a hexagonal CO layer forming a moiré structure, but by multiple diffraction at the substrate and the quasi-hexagonal cluster lattice.

In the classification of high-coverage CO structures on hexagonally close-packed transition metal surfaces the structure belongs to the class of cluster models. It differs from ideal cluster models by the incommensurability with the substrate lattice, which is a result of the variations of the sizes and shapes of the clusters. The fact that the CO layer does not form a mixed sites or moiré structure can be explained by the relatively high energy difference of 0.3 eV between the on-top and the other adsorption sites. That it does not form an antiphase domain boundary structure can be explained by the fact that in these models the molecules can relax from their exact on-top configurations only in one dimension rather than in the two dimensions possible for compact clusters.

Figures

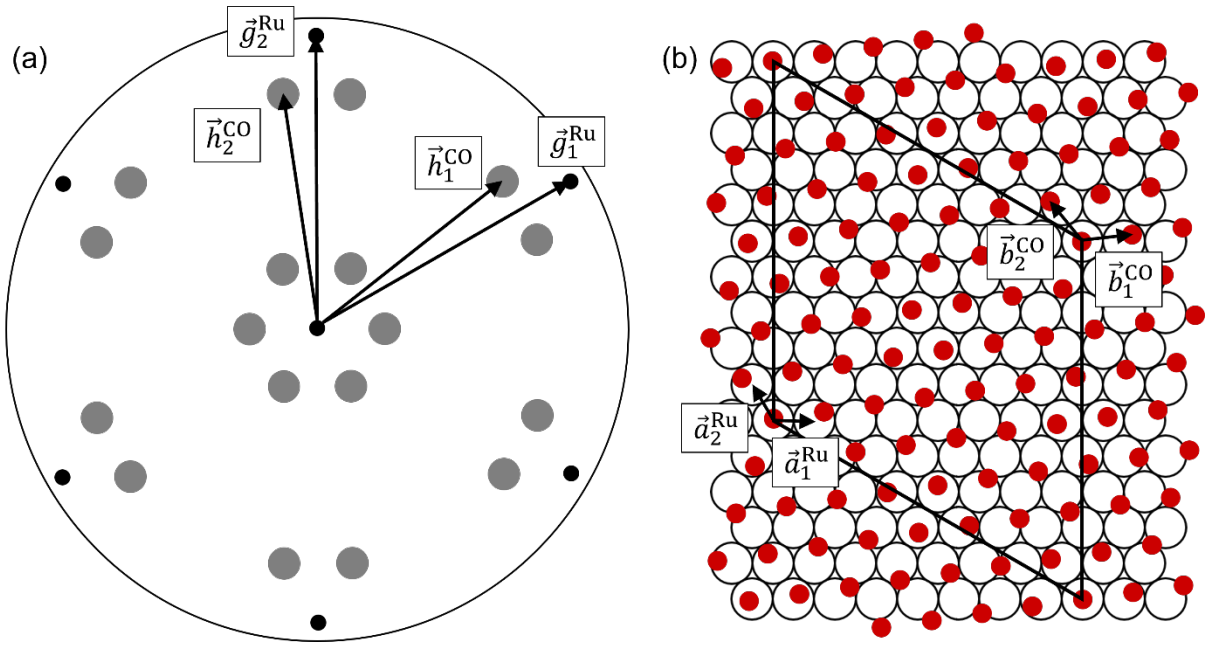

Fig. 1 LEED and moiré model of the saturated CO layer on Ru(0001) from the literature. (a) Schematic LEED pattern, showing the substrate spots (black) and the superstructure spots (grey).[13, 14] $\vec{g}_1^{\mathrm{Ru}}$, $\vec{g}_2^{\mathrm{Ru}}$, $\vec{h}_1^{\mathrm{CO}}$, and $\vec{h}_2^{\mathrm{CO}}$ are the reciprocal basis vectors of the Ru surface and of the hexagonal CO layer, respectively. (b) Previously proposed moiré structure model.[13] $\vec{a}_1^{\mathrm{Ru}}$, $\vec{a}_2^{\mathrm{Ru}}$, $\vec{b}_1^{\mathrm{CO}}$, and $\vec{b}_2^{\mathrm{CO}}$ are the real-space basis vectors of the Ru surface and of the CO layer, respectively, and the rhombus is the unit cell of the $\left(5\sqrt{3}\ x\ 5\sqrt{3}\right)R30°$ structure that had been derived from the LEED pattern.

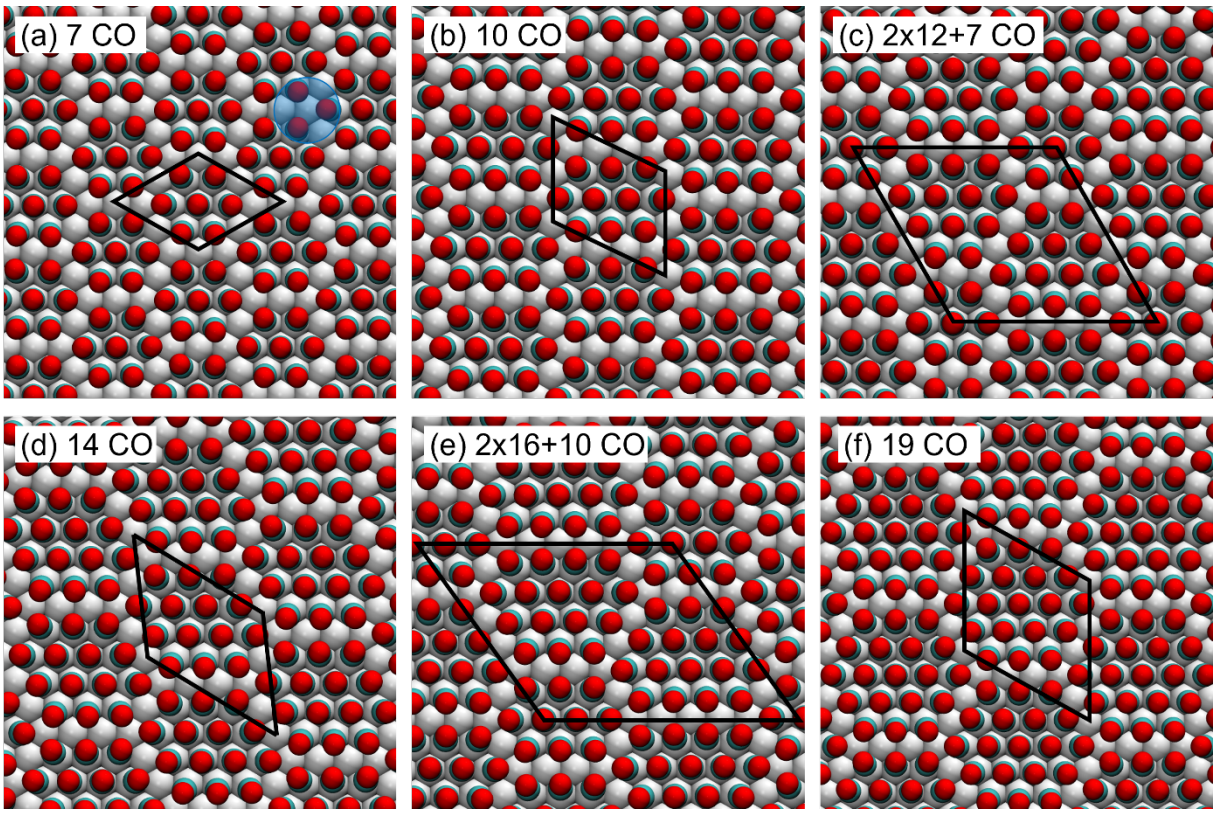

Fig. 2 Structures of the first six cluster models (model type 1) analyzed by DFT. Red balls are the O atoms, petrol balls are the C atoms, grey balls are the Ru atoms, black rhombuses are the unit cells. The blue circle in (a) marks a CO triangle. Coverages: (a) 0.583 ML, (b) 0.625 ML, (c) 0.633 ML, (d) 0.667 ML, (e) 0.667 ML, (f) 0.704 ML.

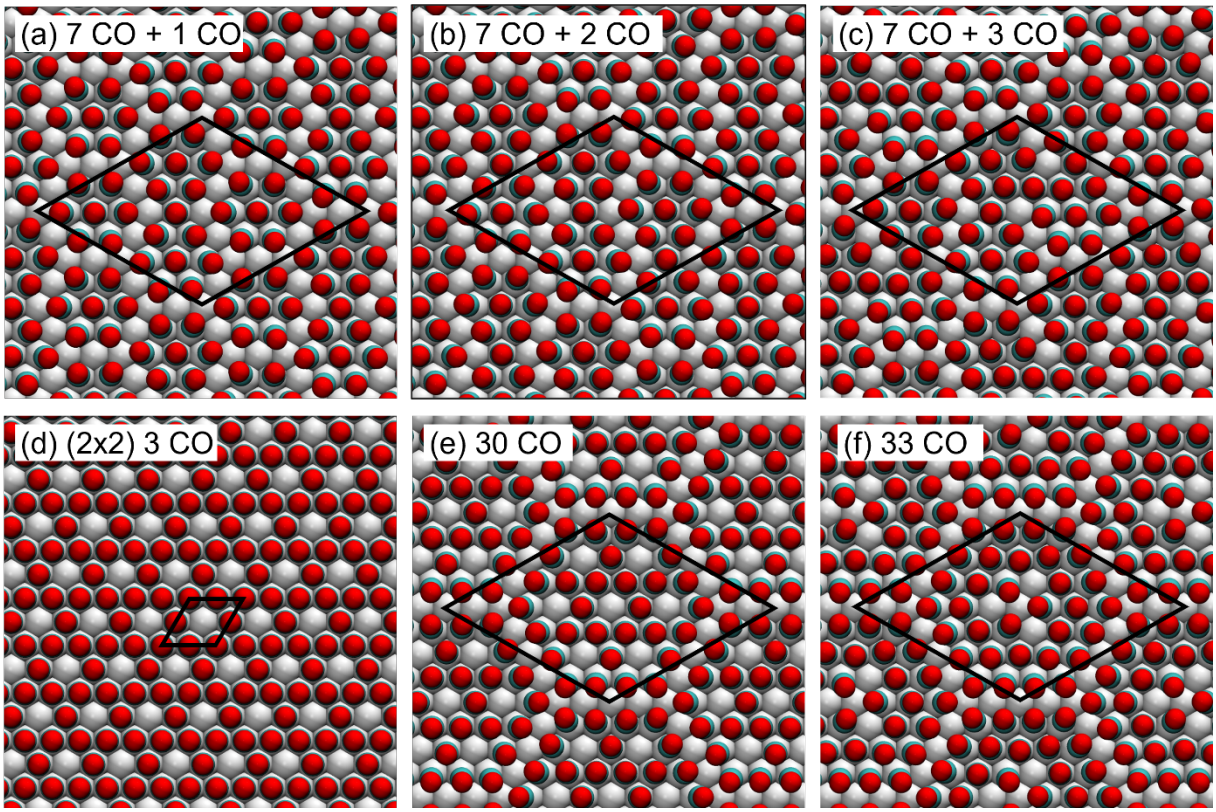

Fig. 3 Structures of model types 2 and 3 analyzed by DFT. Color code as in fig. 2. (a), (b), and (c) are structures of model type 2, with one, two, and three added CO molecules to the $\left(2\sqrt{3}\ x\ 2\sqrt{3}\right)R30°$ structure. Coverages: (a) 0.604, (b) 0.625 ML, (c) 0.646 ML. (d), (e), and (f) are structures and modified structures of model type 3. Coverages: (d) 0.750 ML, (e) 0.625 ML, (f) 0.688 ML.

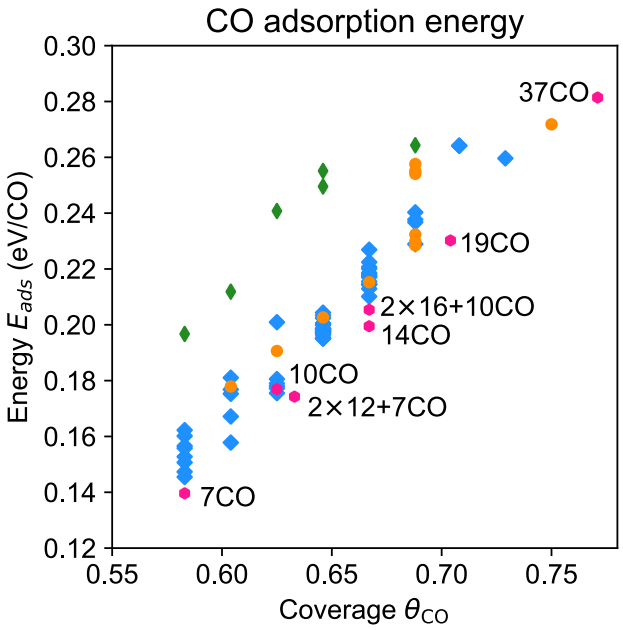

Fig. 4 CO adsorption energies of CO calculated for the three models investigated by DFT as a function of the CO coverage. The values are relative to the adsorption energy of an isolated adsorbed CO molecule. Pink hexagons: model type 1; blue squares: model type 2: green diamonds: model type 3; orange dots: modified type 3 model.

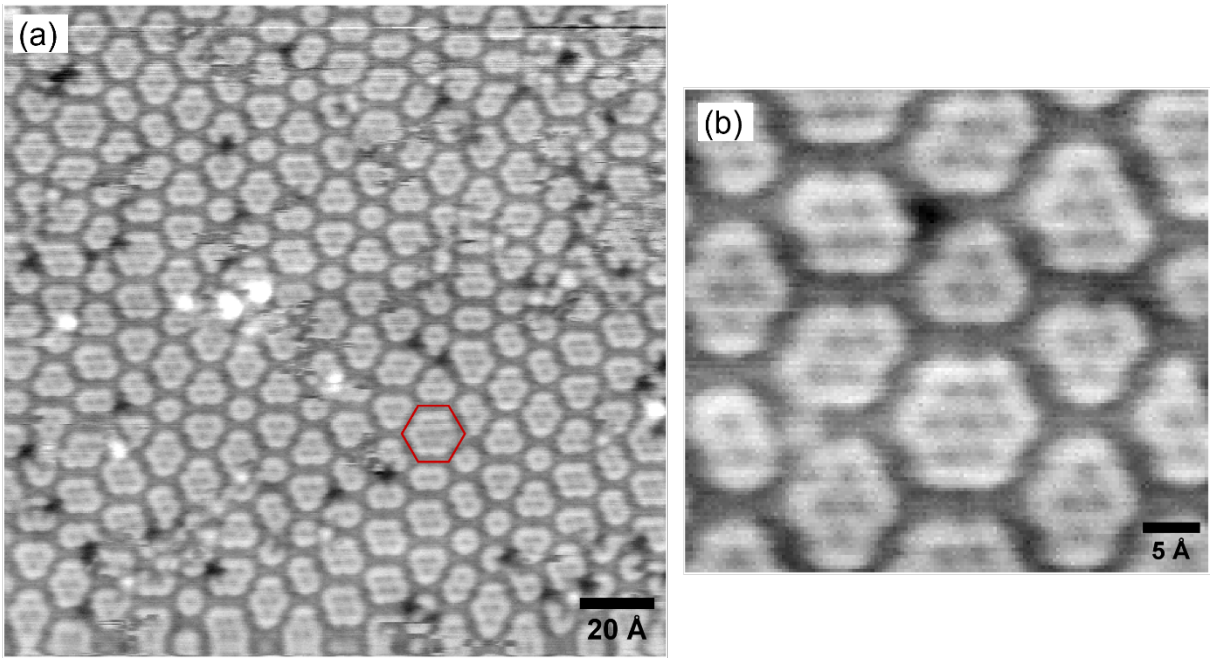

Fig. 5 STM images of the high-coverage CO structure on Ru(0001). (a) Constant current STM image of the CO saturated surface at 62 K. Tunneling voltage (V_t) -1.0 V, tunneling current (I_t) 1 nA, 178 Å x 175 Å. The few small black spots are some N or O atoms. (b) Detail of a constant current STM image of the CO saturated surface at 62 K. V_t = -1.0 V, I_t = 1 nA, 49 Å x 46 Å.

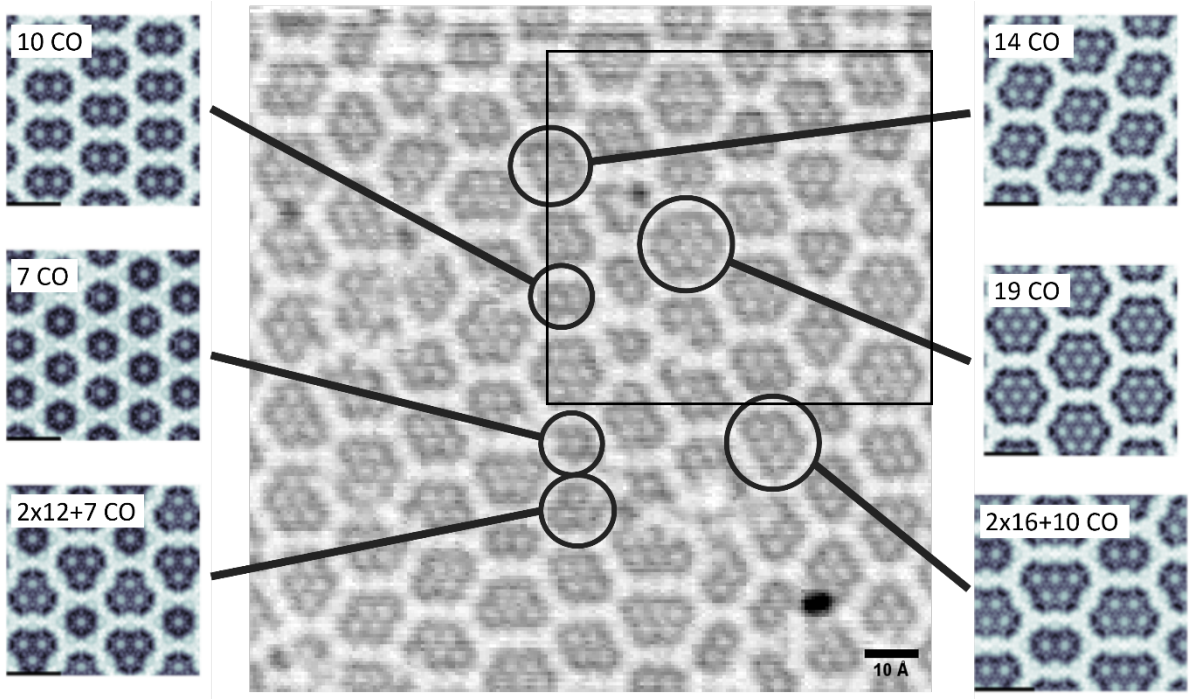

Fig. 6 STM image and comparison with simulated images. Center: Constant height STM image of the CO-saturated surface at 62 K. V_t = -1.4 V, I_t = 3 nA, 126 Å x 126 Å. Outer panels: Simulated constant height images for the six structure models of fig. 2 (integration range 0.0 to -1.0 eV, distance from the O atoms 2.5 Å). The black rectangle is the region shown in fig. 7.

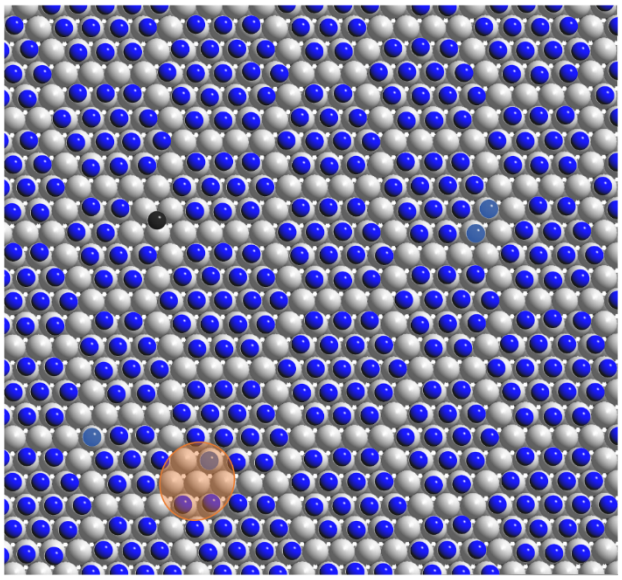

Fig. 7 Model of the CO layer on the Ru(0001) surface at saturation (black rectangular region in fig. 6). Blue balls are CO molecules, grey balls are the Ru atoms. Shown in light blue are some CO molecules the positions of which are unclear. The orange circle marks an area where the CO molecules do not form a triangle configuration. The STM image (fig. 6) shows instabilities in this area.

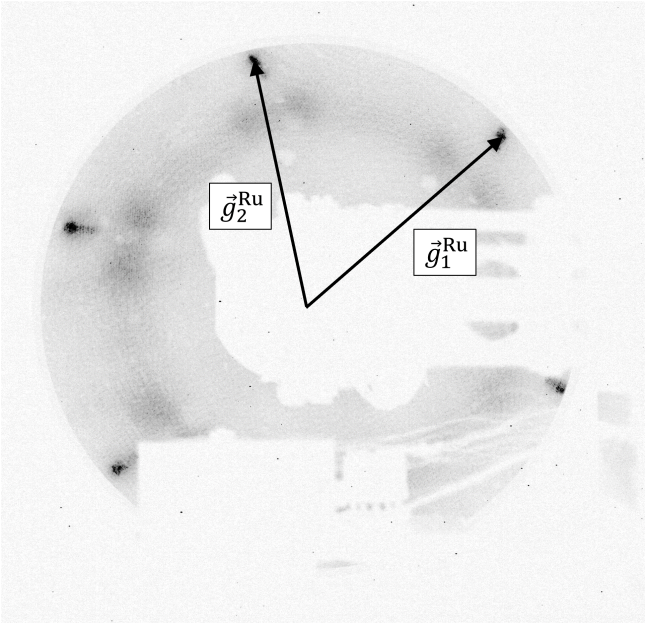

Fig. 8 LEED pattern of the CO-saturated Ru(0001) surface. Electron energy 50 eV, T = 150 K. The splitting of the substrate spots results from a defect in the electron gun. $\vec{g}_1^{\mathrm{Ru}}$, $\vec{g}_2^{\mathrm{Ru}}$ are the reciprocal basis vectors of the Ru surface. The six spots close to the origin are behind the manipulator.

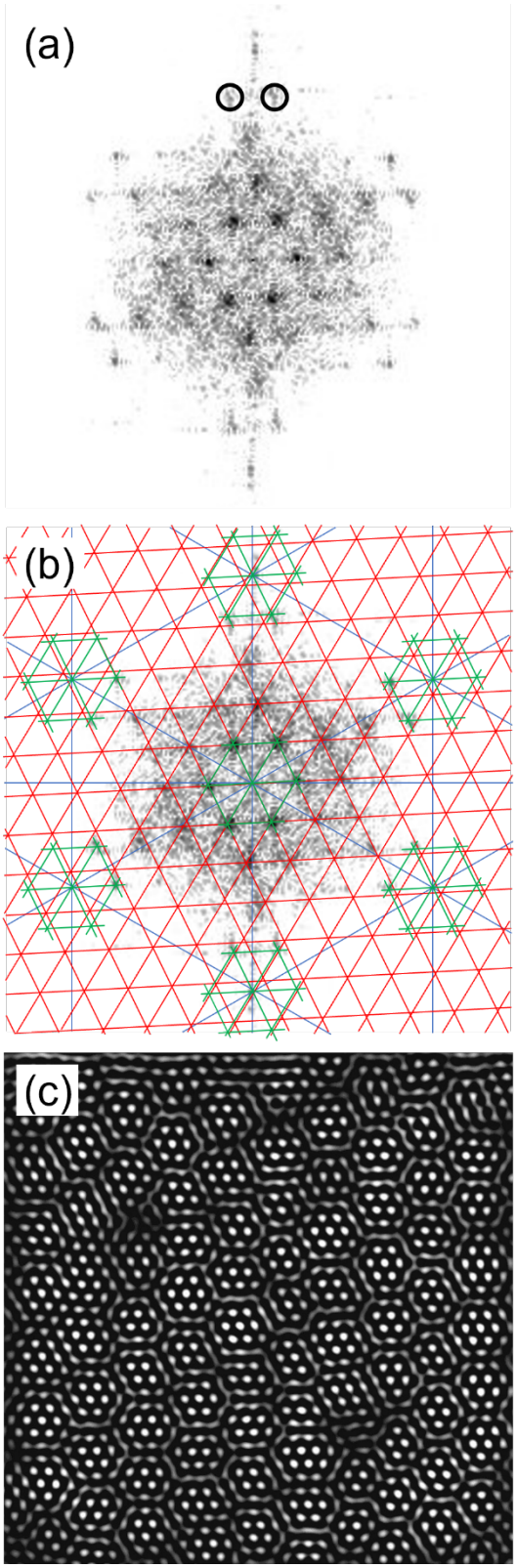

Fig. 9 Fourier analysis of the STM data. (a) Fourier transform of the constant height STM image of fig. 6. The two marked spots are displaced from the lattice defined by the inner spots. (b) Same Fourier transform as in (a) with superimposed line grids. Red line grid: Reciprocal lattice of the cluster pattern, blue line grid: Reciprocal lattice of the substrate, green hexagons: First order spots of the cluster pattern. (c) Fourier back transformation of the combined marked spots in (a) and equivalents.

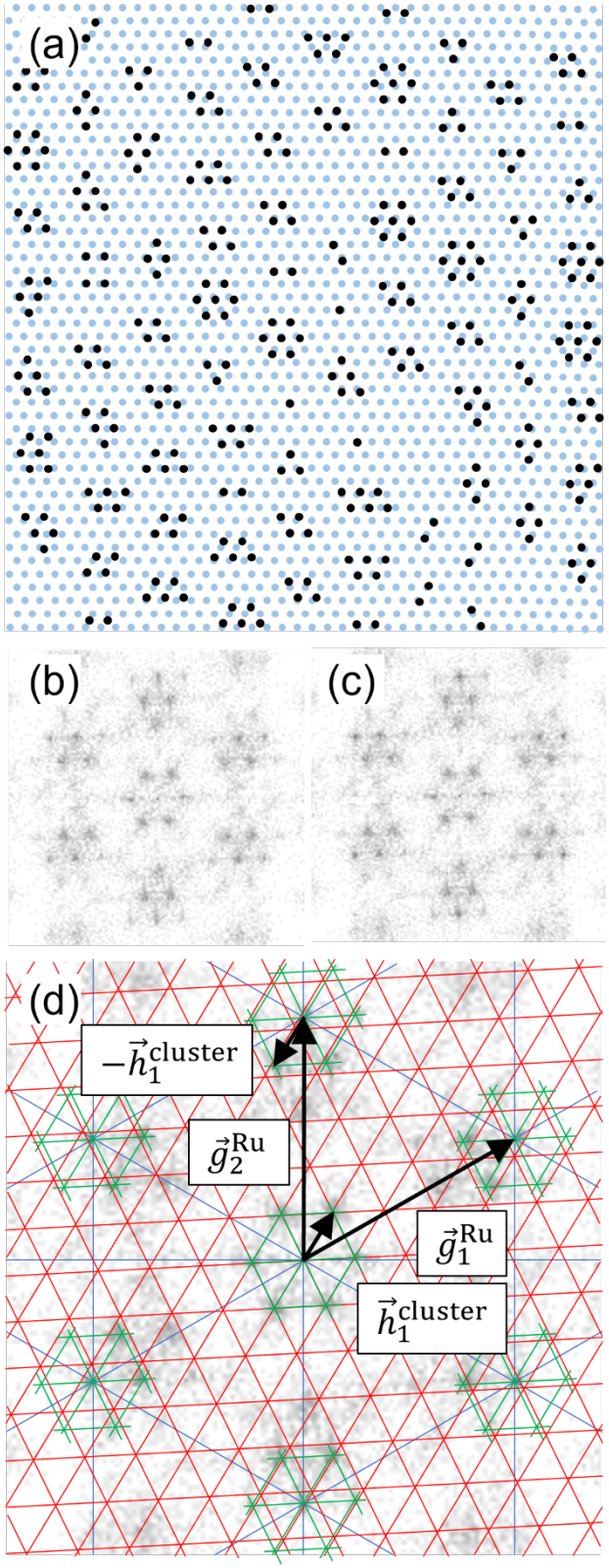

Fig. 10 Fourier analysis of a dot model. (a) Dot model of the STM image of fig. 6. Black dots are the positions of the dots of the internal fine structure of the clusters; blue dots are the Ru atoms of the reconstructed substrate. (b) Fourier transform of the black dots in (a), without the blue dots. (c) Fourier transform of the black dots together with the blue dots. (d) Fourier transform of (b) with superimposed line grid. $\vec{g}_1^{\text{Ru}}$ and $\vec{g}_2^{\text{Ru}}$ are the reciprocal basis vectors of the substrate, and $\vec{h}_1^{\text{cluster}}$ is a reciprocal basis vector of the quasi-hexagonal cluster lattice. Color code as in fig. 9(b).

Acknowledgments

This work has been supported by the Dr. Barbara Mez-Starck Foundation; computer time has been provided by the state of Baden-Württemberg through bwHPC and the German Research Foundation (DFG) under grant no INST 40/575-1 FUGG (JUSTUS 2 cluster).

Author Declarations

Conflict of Interest

The authors have no conflicts to disclose.

Author Contributions:

Hannah Illner: Conceptualization (equal); Investigation (equal); Visualization (equal); Writing – original draft (equal); Writing – review and editing (equal). **Sung Sakong**: Conceptualization (equal); Funding Acquisition (equal?); Investigation (equal); Visualization (equal); Writing – review and editing (equal). **Axel Groß**: Funding Acquisition (equal?); Supervision (?); Writing – review and editing (equal). **Joost Wintterlin**: Conceptualization (equal); Supervision (?); Writing – original draft (equal); Writing – review and editing (equal).

Data Availability

The data that supports the findings of this study are available from the corresponding author upon reasonable request. The optimized atomic coordinates of the DFT calculations are openly available in Zenodo at https://doi.org/10.5281/zenodo.10784616.

Highlight Image

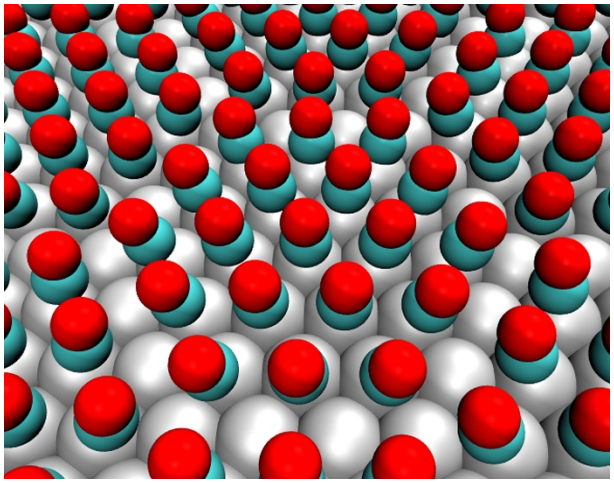

References

1. B. Böller, P. Zeller, S. Günther and J. Wintterlin, ACS Catal. **10**, 12156-12166 (2020).
2. S. R. Longwitz, J. Schnadt, E. K. Vestergaard, R. T. Vang, I. Stensgaard, H. Brune and F. Besenbacher, J. Phys. Chem. B **108**, 14497-14502 (2004).
3. J. P. Biberian and M. A. Van Hove, Surf. Sci. **138**, 361-389 (1984).
4. V. Sumaria, L. Nguyen, F. F. Tao and P. Sautet, ACS Catal. **10**, 9533-9544 (2020).
5. H. Froitzheim, H. Hopster, H. Ibach and S. Lehwald, Appl. Phys. **13**, 147-151 (1977).
6. W. Braun, H. P. Steinrück and G. Held, Surf. Sci. **575**, 343-357 (2005).
7. M. Tüshaus, W. Berndt, H. Conrad, A. M. Bradshaw and B. Persson, Appl. Phys. A **51**, 91-98 (1990).
8. H. J. Yang, T. Minato, M. Kawai and Y. Kim, J. Phys. Chem. C **117**, 16429-16437 (2013).
9. C. J. Weststrate and J. W. Niemantsverdriet, J. Catal. **408**, 142-154 (2022).
10. K. Ueda, K. Suzuki, R. Toyoshima, Y. Monya, M. Yoshida, K. Isegawa, K. Amemiya, K. Mase, B. S. Mun, M. A. Arman, E. Grånäs, J. Knudsen, J. Schnadt and H. Kondoh, Top. Catal. **59**, 487-496 (2016).
11. Q. Chen, J. Liu, X. Zhou, J. Shang, Y. Zhang, X. Shao, Y. Wang, J. Li, W. Chen, G. Xu and K. Wu, J. Phys. Chem. C **119**, 8626-8633 (2015).
12. H. Illner, S. Sakong, A.-K. Henß, A. Groß and J. Wintterlin, J. Phys. Chem. C **127**, 7197-7210 (2023).
13. E. D. Williams and W. H. Weinberg, Surf. Sci. **82**, 93-101 (1979).
14. H. Pfnür and H. J. Heier, Ber. Bunsenges. Phys. Chem. **90**, 272-277 (1986).
15. G. E. Thomas and W. H. Weinberg, J. Chem. Phys. **70**, 1437-1439 (1979).
16. H. Pfnür, D. Menzel, F. M. Hoffmann, A. Ortega and A. M. Bradshaw, Surf. Sci. **93**, 431-452 (1980).
17. M. Scheffler, Surf. Sci. **81**, 562-570 (1979).
18. P. He, H. Dietrich and K. Jacobi, Surf. Sci. **345**, 241-246 (1996).
19. J.-S. McEwen and A. Eichler, J. Chem. Phys. **126**, 094701 (2007).
20. W. Riedl and D. Menzel, Surf. Sci. **163**, 39-50 (1985).
21. B. A. J. Lechner, X. Feng, P. J. Feibelman, J. I. Cerdá and M. Salmeron, J. Phys. Chem. B **122**, 649-656 (2018).
22. A. K. Henß, J. Wiechers, R. Schuster, V. Platschkowski and J. Wintterlin, Jpn. J. Appl. Phys. **59**, SN1007 (2020).
23. D. W. Goodman and J. M. White, Surf. Sci. **90**, 201-203 (1979).
24. M. J. van Staden and J. P. Roux, Appl. Surf. Sci. **44**, 259-262 (1990).
25. S. Marchini, S. Günther and J. Wintterlin, Phys. Rev. B **76**, 075429 (2007).
26. G. Kresse and J. Furthmüller, Phys. Rev. B **54**, 11169-11186 (1996).
27. B. Hammer, L. B. Hansen and J. K. Nørskov, Phys. Rev. B **59**, 7413-7421 (1999).
28. P. E. Blöchl, Phys. Rev. B **50**, 17953-17979 (1994).
29. S. Grimme, J. Antony, S. Ehrlich and H. Krieg, J. Chem. Phys. **132**, 154104 (2010).
30. D. Mahlberg, S. Sakong, K. Forster-Tonigold and A. Groß, J. Chem. Theory Comput. **15**, 3250-3259 (2019).
31. J. Tersoff and D. R. Hamann, Phys. Rev. B **31**, 805-813 (1985).
32. D. E. Starr and H. Bluhm, Surf. Sci. **608**, 241-248 (2013).
33. S. Günther, P. Zeller, B. Böller and J. Wintterlin, ChemPhysChem **22**, 870-884 (2021).